analytical chemistry

pubs.acs.org/ac Article

# Gas-Phase Ion/Ion Reactions to Enable Radical-Directed Dissociation of Fatty Acid Ions: Application to Localization of Methyl Branching

De'Shovon M. Shenault, Kimberly C. Fabijanczuk, Rayan Murtada, Shane Finn, L. Edwin Gonzalez, Jinshan Gao,* and Scott A. McLuckey*

Cite This: *Anal. Chem.* 2024, 96, 3389−3401 Read Online

ACCES$ Metrics & More | Article Recommendations | Supporting Information

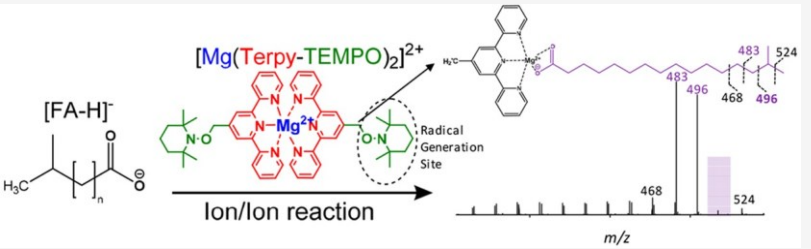


ABSTRACT: Methyl branching on the carbon chains of fatty acids and fatty esters is among the structural variations encountered with fatty acids and fatty esters. Branching in fatty acid/ester chains is particularly prominent in bacterial species and, for example, in vernix caseosa and sebum. The distinction of branched chains from isomeric straight-chain species and the localization of branching can be challenging to determine by mass spectrometry (MS). Condensed-phase derivatization strategies, often used in conjunction with separations, are most commonly used to address the identification and characterization of branched fatty acids. In this work, a gas-phase ion/ion strategy is presented that obviates condensed-phase derivatization and introduces a radical site into fatty acid ions to facilitate radical-directed dissociation (RDD). The gas-phase approach is also directly amenable to fatty acid anions generated via collision-induced dissociation from lipid classes that contain fatty esters. Specifically, divalent magnesium complexes bound to two terpyridine ligands that each incorporate a ((2,2,6,6-tetramethyl-1-piperidine-1-yl)oxy) (TEMPO) moiety are used to charge-invert fatty acid anions. Following the facile loss of one of the ligands and the TEMPO group of the remaining ligand, a radical site is introduced into the complex. Subsequent collision-induced dissociation (CID) of the complex exhibits preferred cleavages that localize the site(s) of branching. The approach is illustrated with *iso*-, *anteiso*-, and isoprenoid branched-chain fatty acids and an intact glycerophospholipid and is applied to a mixture of branched- and straight-chain fatty acids derived from *Bacillus subtilis*.



## INTRODUCTION

Fatty acids (FAs) constitute an important class of lipids that fulfill various physiological functions,[1−3] and fatty acid esters (FAEs) are present in multiple major lipid classes (e.g., di- and triacylglycerols, glycerophospholipids (GPLs), etc.) A variety of FA and FAE structural types can be found in living systems including, for example, straight-chain saturated species of varying chain lengths, unsaturated chains with both *cis* and *trans* configurations, substituted chains, and branched chains. Branching sites, which are most commonly located near the terminal end of the carbon chain,[4] are classified as *iso*-, *anteiso*-, multimethyl-, or *ω*-alicyclic.[5] Branching is common in many bacterial species.[6] For example, up to 75% of the total fatty acid content of *Bacillus subtilis* has been reported to be composed of branched species.[7−9] While branching is common in many genera of bacteria, branched fatty acids (25% by weight) can be found naturally in vernix caseosa (the secretion covering newborn children)[10,11] and have, for example, been reported in the gastrointestinal tracts of newborns[12] and meibum (present in eye tear film).[13] Indeed, numerous studies of branched fatty acids (such as phytanic acid, pristanic acid, and valproic acid (VPA)) focus on understanding the biochemical and physiological roles that BCFAs play in humans.[14−18]

The speciation of saturated FAs and FAEs can be challenging in that there can be variations among branching sites in branched species, which are often present with the isomeric straight-chain isomers.[19] Historically, free fatty acid (FFA) analysis has been addressed by converting FFAs to their methyl esters (i.e., fatty acid methyl esters (FAMEs)) followed by gas chromatography mass spectrometry (GC-MS)[20−23] and/or GC-tandem mass spectrometry (GC-MS/MS).[24−26] Derivatization for GC, such as methyl esterification and other

Received: October 7, 2023
Revised: January 17, 2024
Accepted: January 25, 2024
Published: February 14, 2024

forms of derivatization,[27,28] is performed, at least in part, to increase the FA volatility for GC separation. However, electrospray ionization (ESI) allows for the generation of FFA anions, as well as anions from other polar lipids, without a derivatization step and has become the dominant form of ionization in lipidomics.[29−34] ESI is directly compatible with liquid chromatography (LC), and as a result, LC-MS and LC-MS/MS are dominant approaches in lipidomics[35,36] and have been applied to the identification and quantitation of FFAs and FAEs in biological extracts.[37,38] However, low-energy collision-induced dissociation (CID) of deprotonated fatty acids provides little structural information,[39,40] in contrast with high-energy CID.[41]

When the combination of the most widely used ionization and dissociation method fails to provide the structural information of interest, the options for accessing this information are to generate either a different precursor ion type or to employ a different dissociation method (or both).[42] In the case of lipids, so-called "charge switching" strategies that involve either condensed-phase or gas-phase strategies to alter the lipid ion polarity have been used to facilitate structural characterization.[43,44] Many approaches have been described that employ condensed-phase derivatization strategies to enhance the ionization of FFAs in positive ion mode, some of which also allow for structural characterization via low-energy CID. A noteworthy example is the line of work involving derivatization with pyridinium-containing reagents,[45] some of which lead to ions that fragment along the carbon chain to reveal structural information,[46−49] including branching site localization.[50] Approaches that lead to enhanced ionization yields as well as ions that yield structural information are particularly attractive for FFA analysis. Several examples involving derivatization to facilitate charge switching and photodissociation have been reported for the structural characterization of FAs.[51−54] In some cases, the objective of the photodissociation step is to generate a radical site in the analyte to enable radical-directed dissociation (RDD), which has been demonstrated to generate structural information that complements that derived from the dissociation of even-electron lipids.[55] Alternative condensed-phase approaches to enable the generation of radical ions using ESI-generated precursors for the structural characterization of lipids via RDD, including the location of branching, have been reported.[56−58] Condensed-phase derivatization approaches that target the carboxylic acid functional group of FFAs, however, have limited applicability to FA anions generated from the gas-phase CID of anionic lipid species that contain FAEs, such as GPLs. (It is desirable to be able to subject intact GPLs to CID in order to generate headgroup and sn-position information, for example.) FA anions generated via gas-phase CID are, however, amenable to gas-phase charge switching reactions. A recent example directly relevant to branched FA anions is the generation of FAs complexed with magnesium terpyridine complexes via gas-phase ion/ion reaction to yield cations that allow for the distinction of the *anteiso* isomer from the *iso* isomer upon low-energy CID. However, the CID spectra of the *iso* and straight-chain isomers were not highly distinct from one another. The use of LC to separate the latter isomers enabled an approach that could be used to distinguish all three isomers.[59] We note that an alternative gas-phase approach is the exposure of cationized lipids to metastable helium atoms to convert them to radical cations.[60]

In this work, we demonstrate the RDD of branched and straight-chain FA isomers following the gas-phase conversion of even-electron deprotonated FAs to radical cations. This work follows a more general strategy for generating various ion types for lipid characterization using gas-phase ion/ion chemistry.[61] The strategy combines the use of divalent metal complexes for gas-phase charge switching, a general approach that has been demonstrated to facilitate the structural characterization of, *inter alia*, FAs[62,63] and fatty acid chains derived from GPLs[64,65] and cardiolipins,[66] with the incorporation of ((2,2,6,6-tetramethyl-1-piperidine-1-yl)oxy) (TEMPO) on the ligands in the complex. The covalent modification of analyte species with TEMPO has been shown to be effective in generating odd-electron species for the RDD of peptides,[67] carbohydrates,[68,69] and lipids.[63] Here, we generate reagent cations composed of divalent magnesium complexed with two terpyridine ligands modified by the addition of a TEMPO group (referred to herein as Terpy-TEMPO ligands), as described below. Key advantages of the approach are that it is rapid, requiring on the order of hundreds of milliseconds, it is compatible with either shot-gun lipidomics,[70] as demonstrated here, or can be combined with LC, it can provide structural information from FAEs present in a lipid anion (e.g., a deprotonated GPL) or a deprotonated FA anion generated via ESI, and it avoids condensed-phase modifications, which can compromise signal levels and generate a more complex mass spectrum.

## EXPERIMENTAL SECTION

**Nomenclature.** The shorthand notation for lipid structures recommended by Liebisch et al. is used throughout this work.[71] SCFAs are represented by the total number of carbons in the backbone chain before the colon. To indicate methyl branching sites, "Me" is written after the positions of the branching in parentheses. For example, 14-methyl palmitic acid (14-methyl-hexadecanoic acid) is indicated as FA 16:0(14Me). Phytanic acid (3,7,11,15-tetramethylhexadecanoic acid) is indicated as 16:0(3Me,7Me,11Me,15Me).

**Chemicals and Bacteria.** Heptadecanoic acid, 14-methyl palmitic acid (16:0 (14Me)), 15-methyl palmitic acid (16:0 (15Me)), stearic acid, 17-methyl stearic acid methyl ester (18:0 (17Me)), phytanic acid (16:0 (3Me,7Me,11Me,15Me)), and arachidic acid standards were purchased from Cayman Chemical Company (Ann Arbor, MI). 1-(12*S*-methylmyristoyl)-2-(13-methylmyristoyl)-*sn*-glycero-3-phosphoethanolamine (PE 14:0 (12Me)/15:0 (13Me) was purchased from Avanti Polar Lipids, Inc. (Alabaster, AL). Magnesium chloride, HPLC-grade methanol, HPLC-grade water, and chloroform were purchased from Thermo Fisher Scientific (Waltham, MA). Tert-butyl methyl ether (MTBE) were purchased from Sigma-Aldrich, Inc. (St. Louis, MO). *Bacillus subtilis* (ATCC 23857) was purchased from bioMérieux (Hazelwood, MO).

**Synthesis of 2,2′:6′,2″-Terpyridine-TEMPO.** In depth details describing the synthesis are available in the SI, pages S3 and S4. The synthesis of terpyridine-TEMPO (Terpy-TEMPO) was briefly achieved by esterification of 2,2′:6′,2″-terpyridine-4′-carboxylic acid, reduction of the corresponding ester to a hydroxymethyl group, conversion of the hydroxymethyl group to a bromomethyl group, and finally substitution of the bromine with 2,2,6,6-tetramethylpiperdine-1-oxyl (TEMPO). All of the intermediates along with the final Terpy-TEMPO reagent were characterized by


https://doi.org/10.1021/acs.analchem.3c04510
Anal. Chem. 2024, 96, 3389−3401

Scheme 1. Summary of the Steps Used to Convert $[FA-H]^-$ Analyte Ions to Radical-Containing Analyte Cations via Ion/Ion Reaction and Subsequent CID to Cleave Off the TEMPO Substituent on the Reagent Ion

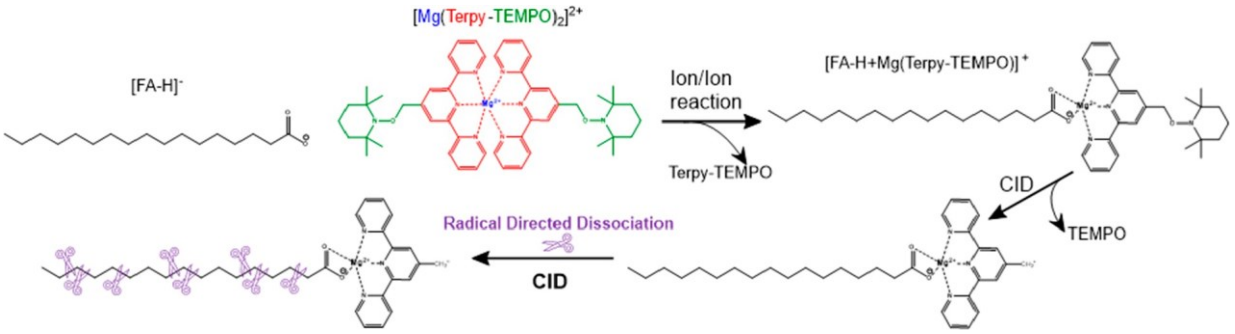


ESI-MS and NMR (NMR spectra are shown in Figures S1–S8).[72−74]

**Sample Preparation.** All lipid standards (free fatty acids and intact GPL) were dissolved in methanol and diluted to a final concentration of 10 μM. Once synthesized and purified, solid Terpy-TEMPO was codissolved with magnesium chloride in a 4:1 (w/w) fashion to an initial stock concentration of ~170:2.50 mM $MgCl_2$:Terpy-TEMPO. The stock solution was diluted to a final concentration of ~170:2.50 μM $MgCl_2$:Terpy-TEMPO. While a 1:2 molar ratio is present in the reagent ion, the use of a 1:2 molar ratio in solution resulted in mostly protonated and sodiated ligand. Thus, it was found that having excess amounts of $MgCl_2$ resulted in an increased level of generation of the desired $[Mg(Terpy\text{-}TEMPO)_2]^{2+}$ reagent.

The following is the procedure used to prepare the bacteria. A 10 μL sample of *Bacillus subtilis* from a glycerolized stock was streaked onto a tryptic soy agar with a 5% sheep's blood (TSAB) agar plate (BBL, BD Diagnostics, Franklin Lakes, NJ) with a 10 μL sterile inoculating loop. The streaked agar plate was incubated in a jar with a lit candle to increase atmospheric $CO_2$ for 24 h at 37 °C. After incubation, the bacteria were carefully scraped from the plates and washed five times with ultrapure water in 2.0 mL Eppendorf tubes. The pelleted bacteria were then vortex mixed in 500 μL of a lysis solvent consisting of isopropanol:acetonitrile:$H_2O$:$CHCl_3$ in a 3:2:2:1 ratio and sonicated for 1 h.[75] The sonicated suspension of lysed bacteria was then pelleted once more, and the supernatant was removed carefully so as not to disturb the pelleted cellular debris. The supernatant of the lysate was then transferred to clean silanized 1.5 mL LC vials (ThermoFisher Scientific, Waltham, MA, USA).

**Mass Spectrometry.** Experiments were performed on a Sciex 5600 hybrid quadrupole/time-of-flight tandem mass spectrometer modified for ion/ion reaction studies.[76] Oppositely charged ions were generated and admitted into the collision cell, q2, in alternating fashion.[77] Lipid anions, $[FA - H]^-$, were generated using nano-ESI (−1200 V), mass selected in Q1, and transferred to q2 for storage. Next, the doubly charged cationic complex, $[Mg(Terpy\text{-}TEMPO)_2]^{2+}$, was produced by nano-ESI (+1200 V), mass isolated by Q1, and transferred to q2 to be mutually stored with the $[FA - H]^-$ anions for 30 ms. All of the subsequent $MS^n$ steps were performed in Q2, followed by time-of-flight mass analysis. The two activation methods used were single-frequency ion-trap collision-induced dissociation (IT-CID) at q = 0.2 and dipolar direct current (DDC) activation. Unless stated explicitly, all $MS^n$ experiments were performed using IT-CID. The $MS^n$ process for each experiment is listed in the figures and discussion.

## RESULTS AND DISCUSSION

The overall objective in this work is to perform a gas-phase transformation of even-electron deprotonated FAs generated either directly via nESI or via CID of a deprotonated GPL to odd-electron cations that, upon CID, indicate the location of branching if present. We illustrate the proof of concept using FFAs as all of the standards of interest are readily available. The strategy is to incorporate a TEMPO group into the reagent for gas-phase charge inversion. Incorporating the TEMPO group into the reagent obviates modification of the analyte sample. The overall approach is summarized in Scheme 1, which shows the generation of $[FA\text{-}H+MgTerpy\text{-}TEMPO]^+$ from the reaction of $[FA-H]^-$ with $[Mg(Terpy\text{-}TEMPO)_2]^{2+}$ as the first step in the process. Note that one of the Terpy-TEMPO ligands is lost spontaneously when the reactants come together to form a complex. Isolation and ion trap CID of the $[FA\text{-}H+Mg(Terpy\text{-}TEMPO)]^+$ ion result in homolytic cleavage of the $-CH_2-O-$ bond of the TEMPO moiety, leaving behind a nascent free radical site, as illustrated in the second step shown in Scheme 1, thereby creating a distonic radical ion. Intramolecular hydrogen transfer leads to the radical site migrating to the lipid where RDD can occur upon a subsequent CID step (final step in Scheme 1).

The overall process for generating the radical-containing analyte ion is illustrated in Figure 1 for FA = 17:0 (heptadecanoic acid). Figure 1A depicts the positive ion nESI MS1 spectrum of the reagent ion solution containing $[Mg(Terpy\text{-}TEMPO)_2]^{2+}$, which gives rise to the base peak observed at $m/z$ 414.2. Figure 1B shows the postion/ion reaction product ion spectrum resulting from the reaction between $[17{:}0\text{-}H]^-$ ($m/z$ 269.2) and $[Mg(Terpy\text{-}TEMPO)_2]^{2+}$ showing the charge-inverted product $[FA\text{-}H+Mg(Terpy\text{-}TEMPO)]^+$ ($m/z$ 695.1) and residual cationic reagent ($m/z$ 414.2). Figure 1C shows the ion trap CID product ion spectrum of the $[FA\text{-}H+Mg(Terpy\text{-}TEMPO)]^+$ ion showing dominant TEMPO loss to give the radical-containing analyte ion, $[FA\text{-}H+Mg(Terpy\text{-}CH_2\bullet)]^+$ ($m/z$ 539.1).

**Distinction among Isomeric *iso*-, *anteiso*-, and Straight-Chain FAs.** Table 1 lists homolytic bond dissociation energies at 298 K ($BDE_{298}$) for C-H bonds in hydrocarbons relevant to this work[78] and for the secondary C-H bond in propanoic acid,[79] which is relevant to the


https://doi.org/10.1021/acs.analchem.3c04510
Anal. Chem. 2024, 96, 3389−3401

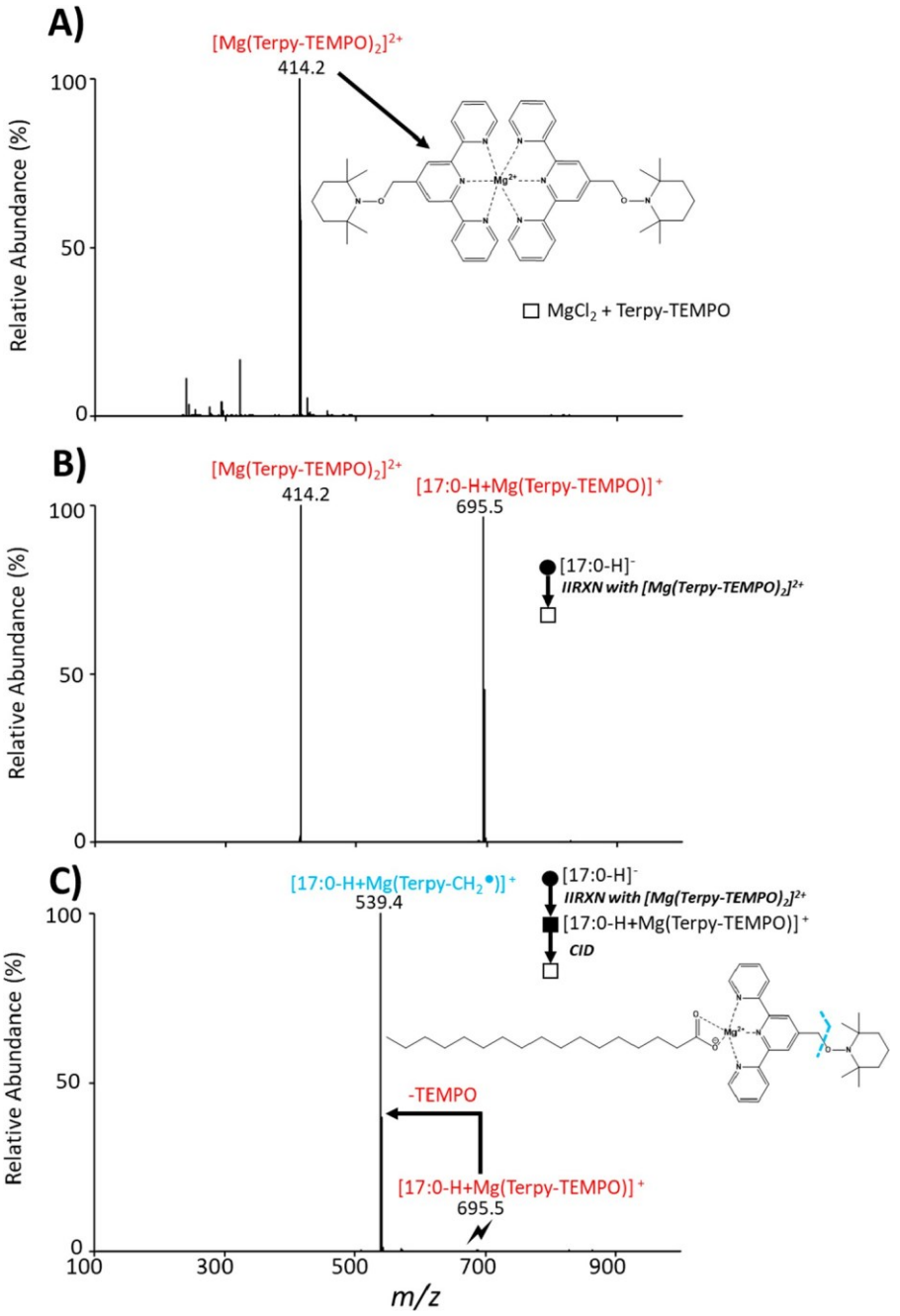


Figure 1. A) MS1$MgCl_2$ + Terpy-TEMPO. B) Postion/ion reaction of $[17:0\text{-}H]^-$ and $[Mg(Terpy\text{-}TEMPO_2]^{2+}$ to yield $[17:0\text{-}H+Mg(Terpy\text{-}TEMPO)]^+$. C) Product ion spectrum of $[17:0\text{-}H+Mg(Terpy\text{-}TEMPO)]^+$ showing the dominant loss of TEMPO. Closed and open circles (●/○) signify selected/unselected anions, respectively, and closed and open squares (■/□) signify selected/unselected cations. The lightning bolt indicates the precursor ion subjected to collisional activation.

Table 1. List of Homolytic Bond Dissociation Energies at 298 K for C-H Bond Types Relevant to This Work

| C-H bond | $BDE_{298}$ (kcal/mol) |
|---|---|
| $C_6H_5CH_2$-H | 89.8 ± 0.6 |
| $C_6H_5$-H | 112.9 ± 0.5 |
| $CH_3CH_2$-H | 101.1 ± 0.4 |
| $(CH_3)_2$CH-H | 98.6 ± 0.4 |
| $(CH_3)_3$C-H | 96.5 ± 0.4 |
| $(CH_3)(CO_2H)$CH-H | 94.3[79] |

methylene adjacent to the carboxylate group. The table lists the $BDE_{298}$ for a benzylic C-H bond to represent the benzylic carbon generated from the loss of TEMPO, an aromatic C-H bond to represent sites on the aromatic groups on the Terpy ligand, the primary, secondary, and tertiary C-H bonds to represent the sites on a deprotonated BCFA within the chain, and the secondary C-H bond adjacent to the carboxylate group of the lipid. It is apparent that hydrogen abstraction by the benzylic carbon generated upon loss of TEMPO is endothermic for all sites, with abstraction from the carbon at


https://doi.org/10.1021/acs.analchem.3c04510
Anal. Chem. 2024, 96, 3389−3401

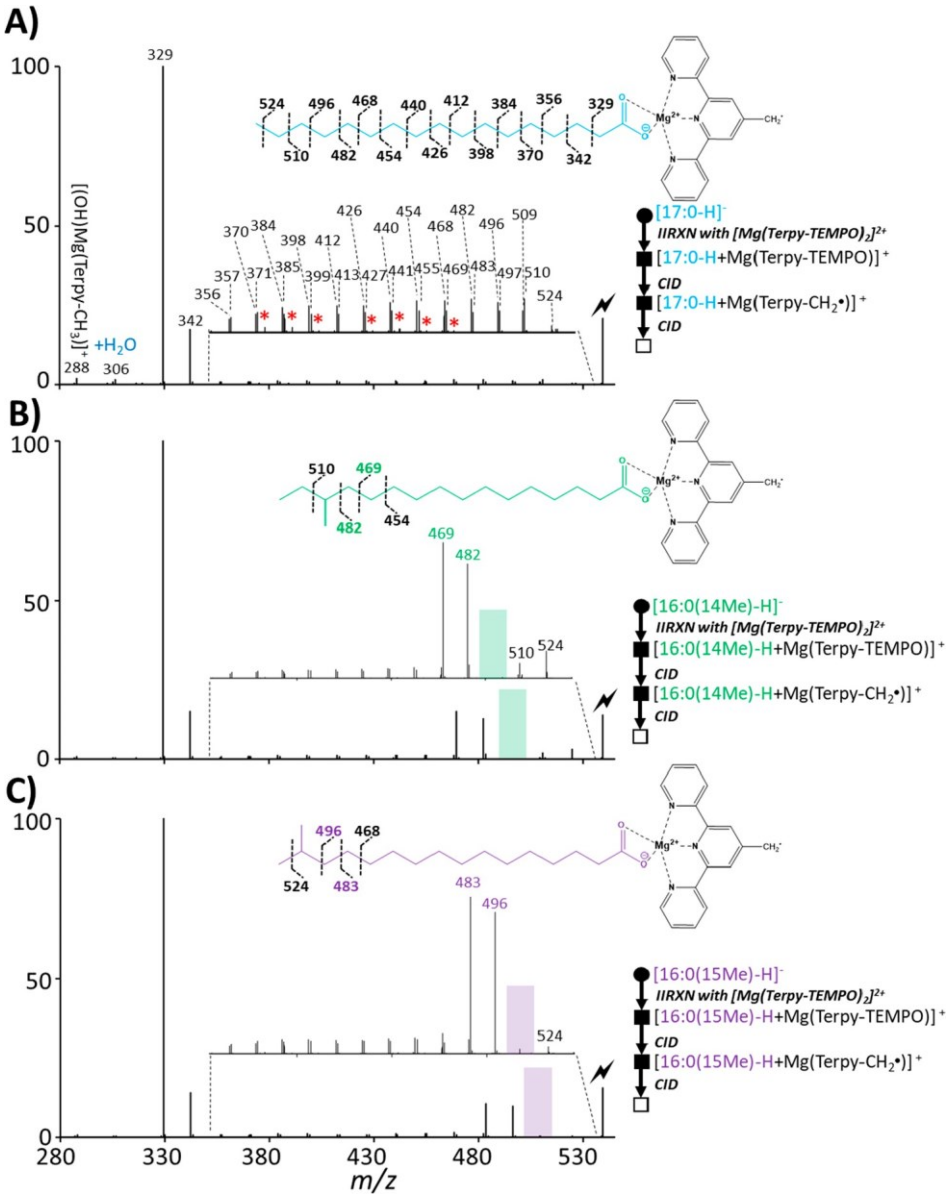


Figure 2. Ion trap CID product ion spectra of A) [17:0-H+MgTerpy-$CH_2$•]$^+$, B) [16:0(14Me)-H+MgTerpy-$CH_2$•]$^+$, and C) [16:0(15Me)-H +MgTerpy-$CH_2$•]$^+$. Closed and open circles (●/○) signify selected/unselected anions, respectively, and closed and open squares (■/□) signify selected/unselected cations. Lightning bolts indicate the precursor ion subjected to collisional activation. Asterisks (*) indicate observed $O_2$ adducts to odd-electron products.[80] While not indicated with asterisks in B) and C) due to the lower *y*-scale expansion, they are also present at low levels.

the C-2 carbon being least endothermic, followed by the branching site (i.e., tertiary C-H).

Figure 2 shows the product ion spectra derived from ion trap CID of the [FA-H+MgTerpy-$CH_2$•]$^+$ ions of three isomeric forms of [17:0-H]$^-$ {i.e., the straight-chain version ([17:0-H +MgTerpy-$CH_2$•]$^+$, Figure 2A), the *anteiso*- version ([16:0-(14Me)-H+MgTerpy-$CH_2$•]$^+$, Figure 2B), and the *iso*- version ([16:0(15Me)-H+MgTerpy-$CH_2$•]$^+$, Figure 2C)} branched versions. For reference, the product ion spectrum of [17:0-H +MgTerpy]$^+$ is provided in Figure S9 to illustrate the charge-remote fragmentation (CRF) behavior observed for an even-electron analog to the ions of Figure 2. For even-electron [FA-H-MgTerpy]$^+$ ions, major lipid product ions correspond to a homolytic cleavage at C-2 to yield [•$H_2$C-$CO_2^-$+MgTerpy]$^+$ at $m/z$ = 314 and alkane loss to give [$H_2$C=$CO_2^-$+MgTerpy]$^+$ at $m/z$ = 328 Da. A series of ions of much lesser abundance with a spacing of 14 Da beginning with the [$H_2$C=CH−$CO_2^-$+MgTerpy]$^+$ product, corresponding to net alkane losses, comprised most of the remaining product ion signal. We also note that when a monoisotopic precursor ion is subjected to activation, ions of only one mass are observed at each carbon number, which indicates that net alkane loss is the exclusive process. The most abundant product ion in Figure S9 corresponds to a hydrolysis product [HOMg(Terpy)]$^+$ at $m/z$ 274, which is commonly observed upon CID of [lipid-H +MgTerpy]$^+$ and [lipid-H+MgPhenanthroline]$^+$ ions.[61−63]

All three of the odd-electron 17-carbon isomer ions show a signal at $m/z$ 288, which is consistent with the addition of the elements of $H_2O$ to [MgTerpy-$CH_2$•]$^+$, which may correspond to [HOMgTerpy-$CH_3$]$^+$, by analogy to the commonly


https://doi.org/10.1021/acs.analchem.3c04510
Anal. Chem. 2024, 96, 3389−3401

Scheme 2. RDD Reactions That Give Rise to the Major Product Ions in Figure 2

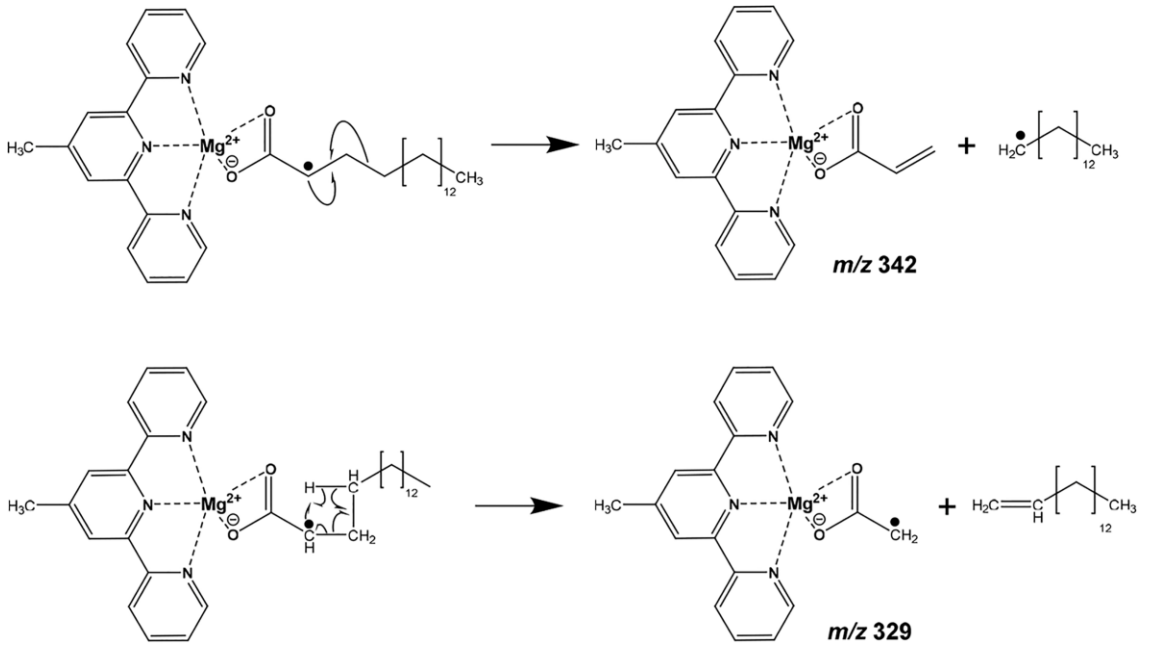


Scheme 3. RDD Reactions Originating from the Branching Site in [16:0(14Me)-H+MgTerpy-$CH_2\bullet$]$^+$

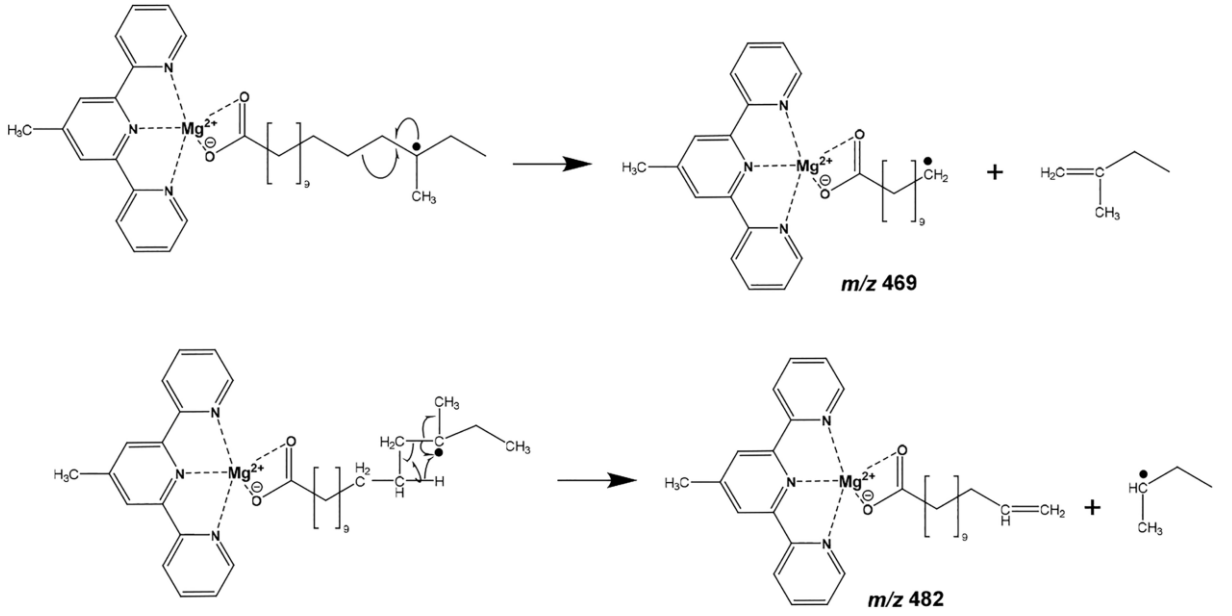


observed [HOMgTerpy]$^+$ ion mentioned above. However, this product is of far lower relative abundance than that with the even-electron precursor ion. The base peak in all cases is observed at $m/z$ 329 Da, which corresponds to a difference in mass of 59 Da relative to [MgTerpy-$CH_2\bullet$]$^+$ (i.e., [$H_3C$-$CO_2^-$+ MgTerpy-$CH_2\bullet$]$^+$) and 58 Da relative to [MgTerpy-$CH_3$]$^+$ (i.e., [$\bullet H_2C$-$CO_2^-$+ MgTerpy-$CH_3$]$^+$). The next most abundant fragment in all three cases appears at $m/z$ 342, which corresponds to [$H_2C$=CH-$CO_2^-$+MgTerpy-$CH_3$]$^+$. A series of very minor products with a 14 Da spacing beginning with $m/z$ 356 is also observed, by analogy to the series of small peaks with a 14 Da spacing seen in Figure S9. However, it is also noteworthy that even when a monoisotopic odd-electron precursor ion is subjected to activation, multiple ions are observed at each carbon number, which indicates the presence of several mechanisms (e.g., alkene and alkyl losses). While contributions from even-electron charge-remote fragmentation mechanisms cannot be precluded, much of what is observed can be rationalized on the basis of RDD. For example, hydrogen transfer from the C-2 carbon of the lipid to the ligand followed by an α-cleavage can give rise to the ion at $m/z$ 342, and a four-centered rearrangement involving hydrogen transfer from the C-4 carbon to the C-2 carbon with concomitant homolytic cleavage of the bond between C-2 and C-3 could give rise to the $m/z$ 329 ion (Scheme 2).


https://doi.org/10.1021/acs.analchem.3c04510
Anal. Chem. 2024, 96, 3389−3401

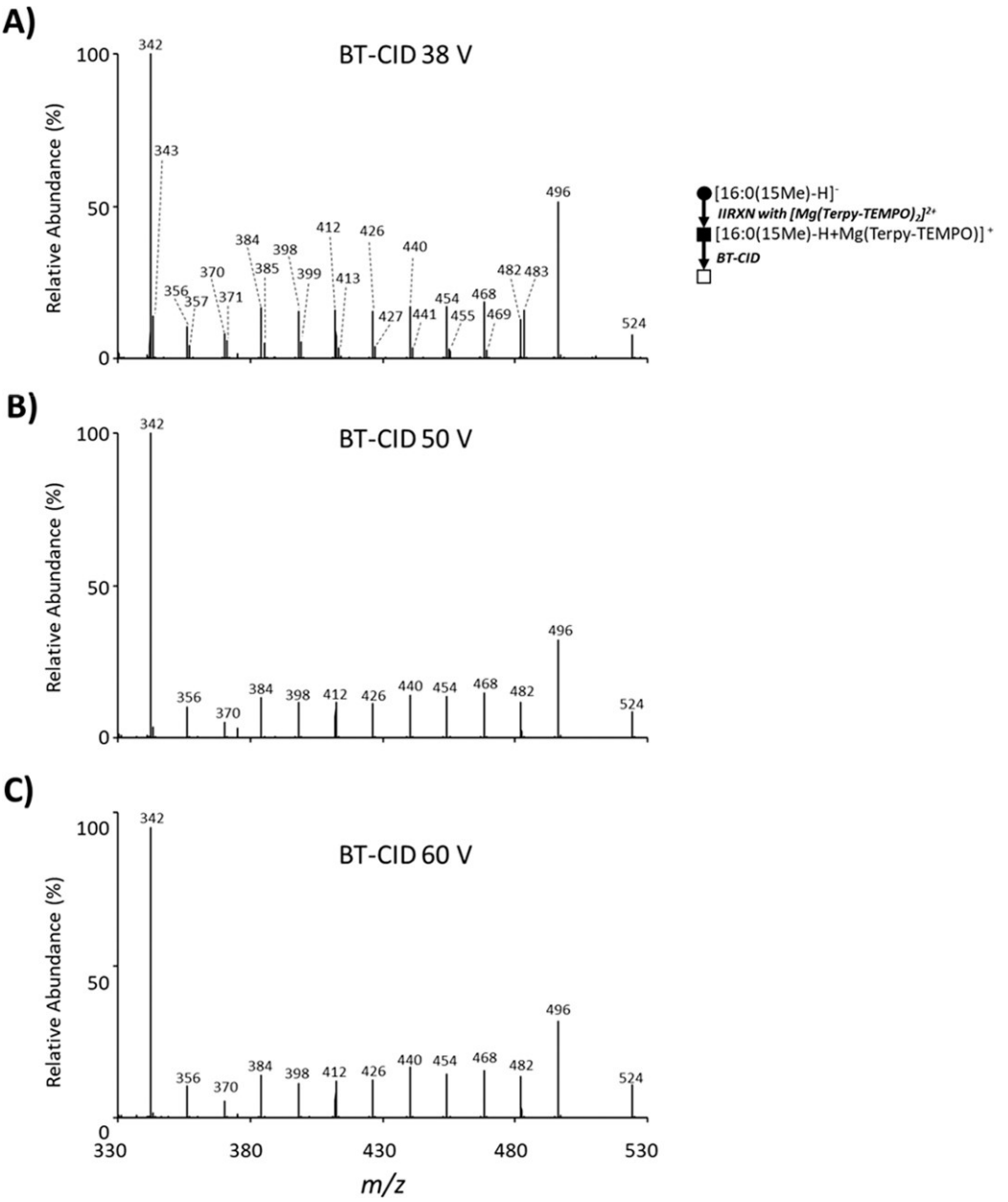


Figure 3. Zoomed-in product ion spectra of [16:0(15Me)-H+MgTerpy-TEMPO]⁺ resulting from ion injection energies into q2 of A) 38, B) 50, and C) 60 eV.

The product ion spectrum of the [16:0(14Me)-H+MgTerpy-$CH_2\bullet$]⁺ isomer (Figure 2B) is essentially identical to that of the straight-chain isomer (Figure 2A) from low $m/z$ up to $m/z$ 468. However, a relatively abundant odd-electron ion at $m/z$ 469 is observed with the branched isomer, which is much more abundant than that observed with the straight-chain isomer. Likewise, a relatively abundant even-electron ion at $m/z$ 482 is apparent in the spectrum of this branched isomer, in contrast to the straight-chain ion. We propose that these ions arise from RDD at the tertiary carbon (C-14) (Scheme 3) via the α-cleavage and four-centered rearrangement mechanisms indicated in Scheme 2. It is also noteworthy that the peak at $m/z$ 496 in the straight-chain isomer is largely missing in the spectrum of the *anteiso*-isomer (Figure 2B), reflecting the site of branching. The behavior of the [16:0(15Me)-H+MgTerpy-$CH_2\bullet$]⁺ isomer (Figure 2C) can be similarly rationalized. The prominent doublet composed of the odd-electron $m/z$ 483 and even-electron $m/z$ 496 ions is consistent with RDD originating from the C-15 position. Furthermore, the diminished signal at $m/z$ 510 is reflective of the site of branching in the *iso*-isomer.

We note that the abundances of the odd-electron products in Figure 2 are more sensitive to activation conditions than are the even-electron products.[81] At high activation energies, for example, odd-electron products may not be observed. The phenomenology is illustrated in Figure S10 and Figure 3, where Figure 3 is a zoom in of Figure S10, which compares the product ion spectra of [16:0(15Me)-H+MgTerpy-TEMPO]⁺ at three different injection energies into q2 (i.e., 38 eV (Figure 3A), 50 eV (Figure 3B), and 60 eV (Figure 3C)). The odd-electron products (see, for example, $m/z$ 483) are essentially


https://doi.org/10.1021/acs.analchem.3c04510
Anal. Chem. 2024, 96, 3389−3401

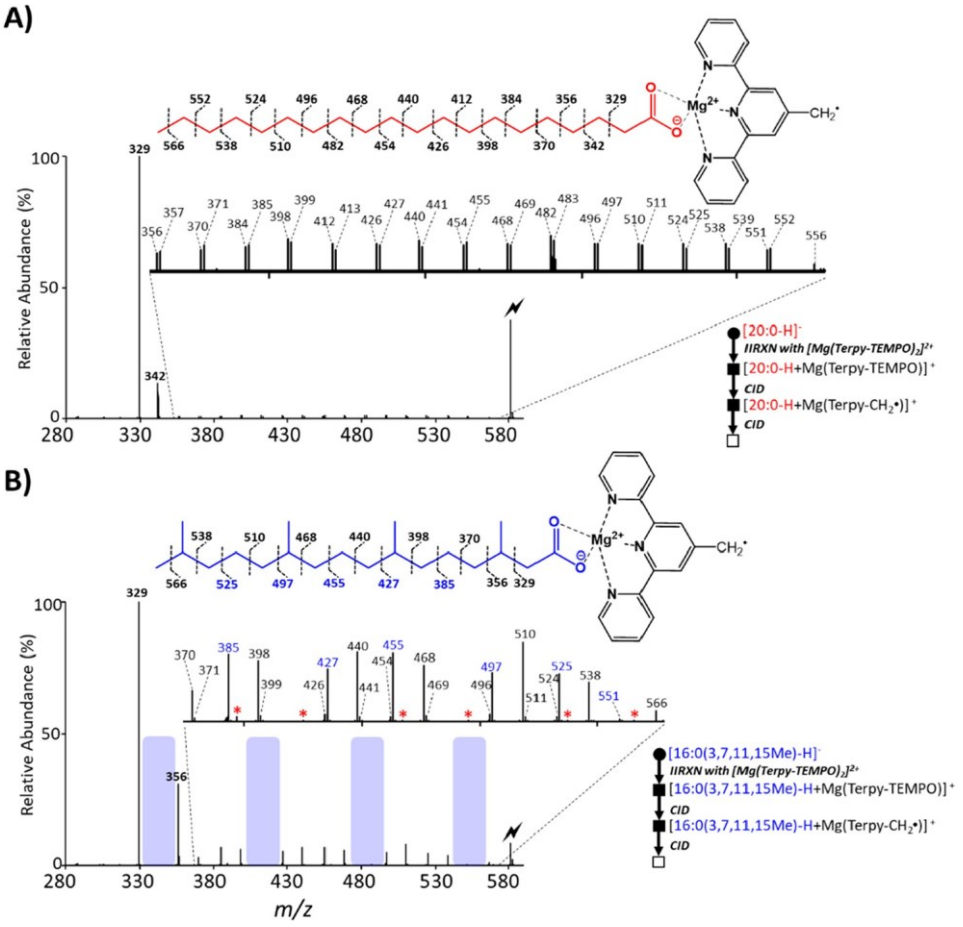


Figure 4. CID product ion spectra of A) [20:0-H+MgTerpy-$CH_2$•]$^+$ and B) [16:0(3,7,11,15Me)-H+MgTerpy-$CH_2$•]$^+$. Closed and open circles (●/○) signify selected/unselected anions, respectively, and closed and open squares (■/□) signify selected/unselected cations. Lightning bolts indicate the precursor ion subjected to collisional activation. Asterisks (*) indicate observed $O_2$ adducts to odd-electron fragment ions.

missing at the two higher collision energies. Experiments using dipolar DC collisional activation[82] clearly showed that the odd-electron ions fragment much more readily than the even-electron counterparts (Figure S11). $MS^n$ experiments showed that the odd-electron products fragment to both even- and odd-electron products, with the most abundant second-generation products falling at $m/z$ 342 and $m/z$ 329 (Figure S12). While the gap in fragmentation that corresponds to the site of branching is not particularly sensitive to collision energy for the *iso*- and *anteiso*-isomers, the prominent doublets observed in Figure 2B and 2C using gentle activation conditions provide a more confident identification of branching sites. Hence, the relatively gentle activation conditions are emphasized here.

We note that FA standards are used to illustrate the ion chemistry associated with the gas-phase charge switching approach. The chemistry is equally applicable to fatty acid anions generated via the CID of fatty ester-containing lipids, such as GPLs. An example is provided in Figure S13, in which CID of PE 14:0 (12Me)/14:0 (13Me) anions yields abundant fatty acid ions at $m/z$ 241 (Figure S13A). In this case, while each fatty acid component has a different branching position, they have identical chemical compositions and thus identical $m/z$ values. Charge inversion of the fatty acid anions was performed with two steps of CID, the first to form the radical via loss of TEMPO and the second to generate fragmentation along the fatty acid chain, revealing the branching positions shown in Figure S13B. The expected "missing" ion for the sn-1 fatty acid chain, 14:0 (12Me), is $m/z$ 468, and the expected "missing" ion for the sn-2 position fatty acid chain, 14:0 (13Me), is $m/z$ 482. A prominent $m/z$ 468 signal is observed, however, due to the contribution of the 14:0 (13Me) ion and its expected prominent signal at $m/z$ 468 from cleavage prior to its' branching position, while only a minor signal at $m/z$ 482 is observed. This implies that the $RCO_2^-$ ion cleaved from sn-2 (i.e., $R_2CO_2^-$) is more abundant than that from sn-1 (i.e., $R_1CO_2^-$), consistent with the literature,[83] where PE anions fragment to form more abundant sn-2 fatty acid ions than sn-1 fatty acid ions.

**Distinguishing Isoprenoid Fatty Acids from Saturated Fatty Acids.** Isoprenoids, derived from isoprene, are a class of branched-chain fatty acids commonly found in plants, microalgae, marine food, bacteria, and fungi that form the backbone of the archaeal membrane of phospholipids. Often considered to be "transportation fuel", isoprenoids can enhance, stabilize, and structure the membrane.[84−86] Common isoprenoids include 4,8,12-trimethyltridecanoic acid, 3,7,11,15-tetramethylhexadecanoic acid (phytanic acid), and 2,6,10,14-tetramethylpentadecanoic acid (pristanic acid). We compare here phytanic acid, 16:0(3,7,11,15Me), with the straight-chain isomer, 20:0, to illustrate the fragmentation behavior of a lipid with multiple branching sites following charge inversion of the


https://doi.org/10.1021/acs.analchem.3c04510
Anal. Chem. 2024, 96, 3389−3401

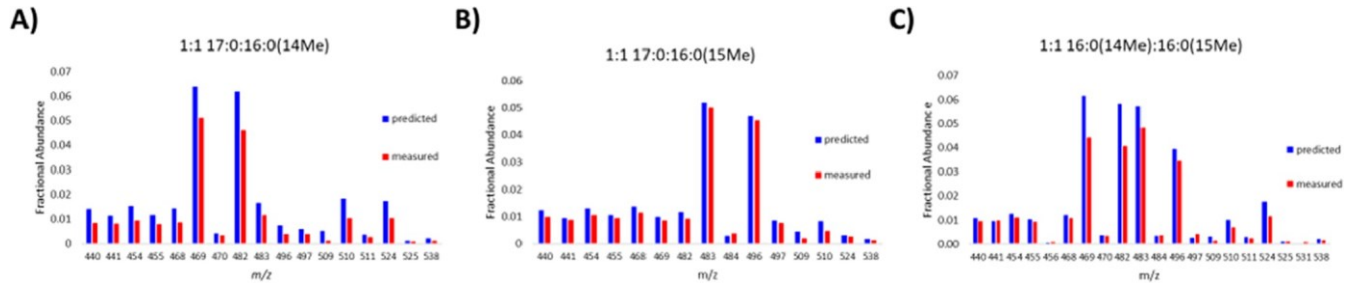


Figure 5. Measured fractional abundances of diagnostic $m/z$ for branching sites for 17:0, 16:0(14Me), and 16:0(15Me). A) 1:1 molar ratio of 17:0:16:0(14Me), B) 1:1 molar ratio of 17:0:16:0(15Me), and C) 1:1 molar ratio of 16:0(14Me):16:0(15Me). Predicted measurements were calculated by linear combinations of pure standards.

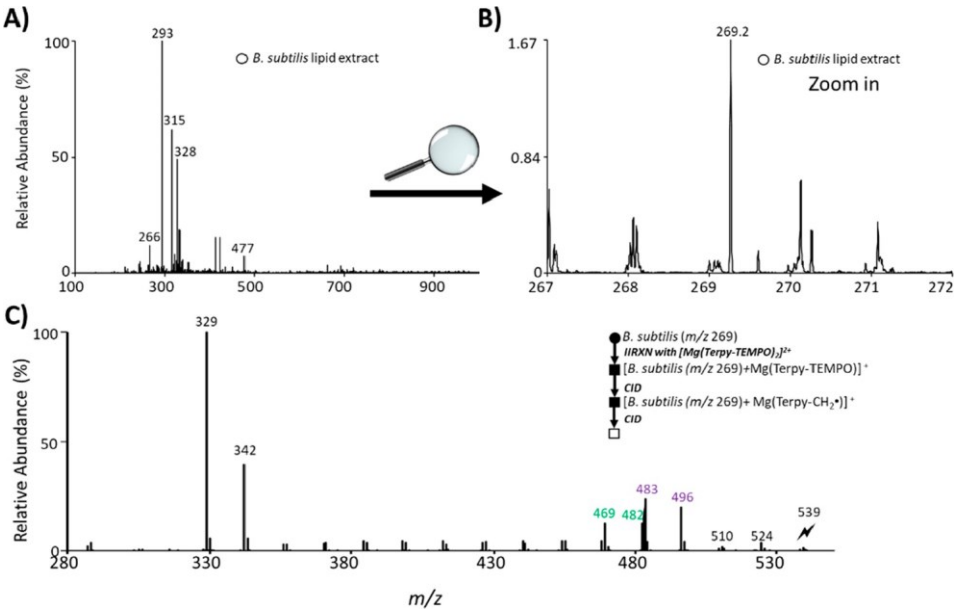


Figure 6. A) MS1 of negative mode nESI of the *B. subtilis* lipid extract, B) zoom in of MS1 from A), and C) CID of $m/z$ 539 generated isolation of $m/z$ 269 from *B. subtilis* lipid extract that was charge-inverted using $[Mg(Terpy\text{-}TEMPO)_2]^{2+}$, with subsequent CID to form the radical species.

respective $[FA\text{-}H]^-$ anions with $Mg(Terpy\text{-}TEMPO)_2^{2+}$. Figure 4 shows the product ion spectra of $[20{:}0\text{-}H+MgTerpy\text{-}CH_2\bullet]^+$ (Figure 4A) and $[16{:}0(3,7,11,15Me)\text{-}H+MgTerpy\text{-}CH_2\bullet]^+$ (Figure 4B). The dominant products are observed at $m/z$ 329 and $m/z$ 342 for the $[20{:}0\text{-}H+MgTerpy\text{-}CH_2\bullet]^+$ precursor ion, by analogy to the results for $[17{:}0\ H+MgTerpy\text{-}CH_2\bullet]^+$ (Figure 2A and Scheme 2). Likewise, a series of ions with 14 Da spacings, reflecting cleavages along the chain, are noted at very low relative abundance.

Fragmentation of the $[16{:}0(3,7,11,15Me)\text{-}H+MgTerpy\text{-}CH_2\bullet]^+$ ion does not show the consistent series of products differing in mass by 14 Da (Figure 4B). Rather, gaps in the spectrum along with patterns of RDD products reveal the locations of the four branching sites. The most likely sites for initial radical formation, based on BDEs (Table 1), are C-2, C-3, C-7, C-11, and C15. The product ions expected from the RDD mechanisms illustrated in Schemes 2 and 3 (i.e., α-cleavage and the four-centered rearrangement) are listed in Table S1 for each of the initial radical sites indicated above. Briefly, the mechanisms shown in Scheme 2 for an initial radical site at C-2 give rise to the product ions at $m/z$ 329 and $m/z$ 356. The 27 Da gap between these ions indicates the presence of a methyl group on C-3. (Otherwise, a major product at $m/z$ 342 would be observed, as it is in Figure 2A.)

With the initial branching site on C-3, the product at $m/z$ 370 can be generated via α-cleavage and the product at $m/z$ 357 can be generated via the four-centered rearrangement. The branching sites in the middle of the chain (i.e., C-7 and C-15) can give rise to a wider array of products because the likelihoods for α-cleavages and four-centered rearrangements are more or less equally probable from either side of the initial radical site. In the case of C-7, for example, product ions at $m/z$ 385 and $m/z$ 440 can be generated via α-cleavages originating at C-7 whereas product ions at $m/z$ 398 and $m/z$ 427 can originate from four-centered rearrangements. See Table S1 for a list of the possible products from the initial radical site at C-11. The major products from the radical site at C-15 are $m/z$ 525 from α-cleavage to give $m/z$ 525 and $m/z$ 538 from the four-centered rearrangement. Note that product ions at all of the $m/z$ values listed here and in Table S1 are observed in Figure 4B and that no ions at $m/z$ values of 342, 412, 482, and 552 are observed. The latter $m/z$ values represent gaps in the spectrum that coincide with the branching sites.

**Relative Quantitation of Straight- and Branched-Chain Fatty Acids in Shot-Gun Analysis of Standards and *Bacillus subtilis*.** The unique fragmentation patterns of straight- and branched-chain fatty acids provide the possibility


https://doi.org/10.1021/acs.analchem.3c04510
Anal. Chem. 2024, 96, 3389−3401

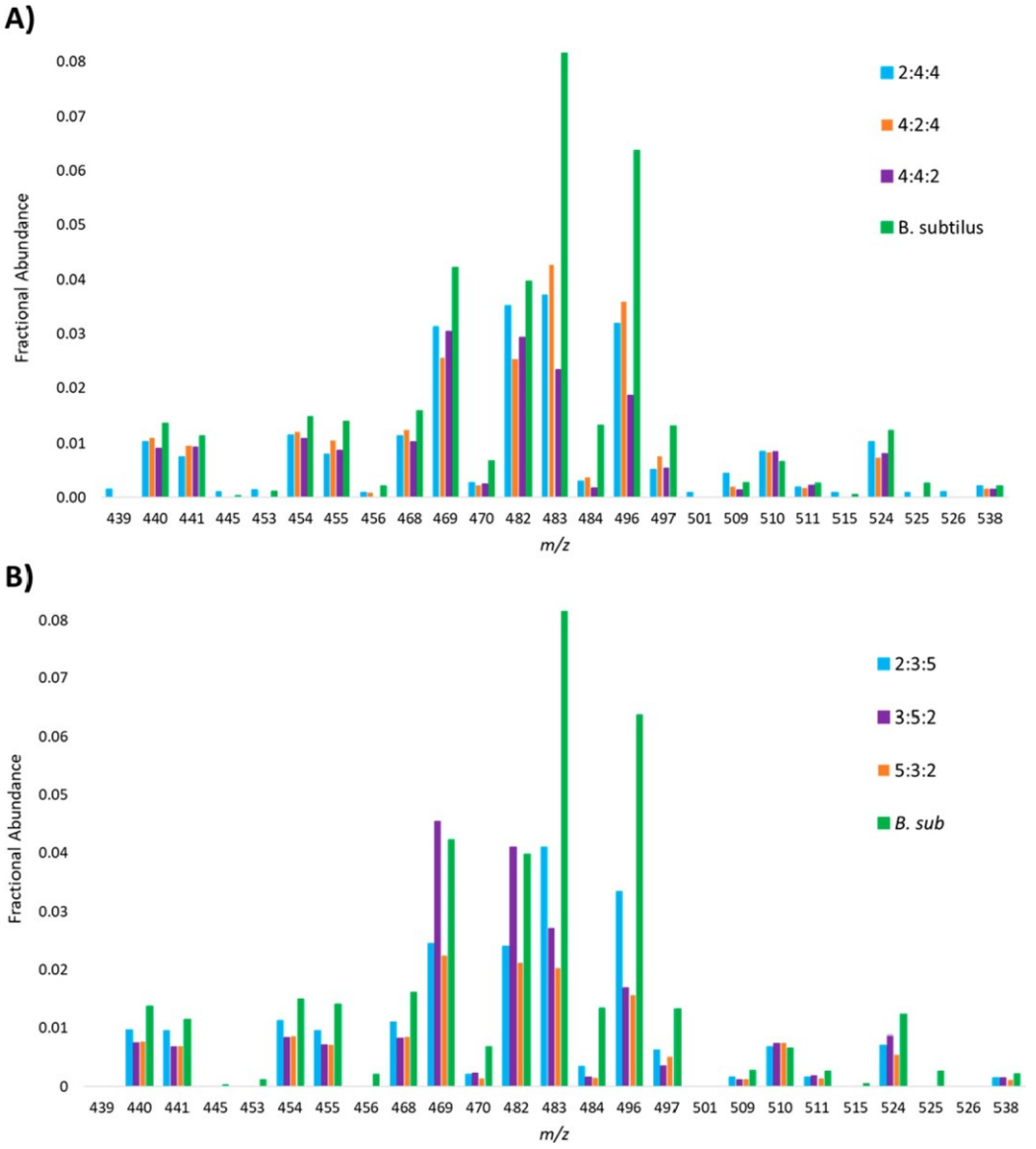


Figure 7. A) and B) Various ratio ternary mixtures of 17:0:16:0(14Me):16:0(15(Me) fractional abundances, with the fractional abundances calculated from the unknown $m/z$ isolated from *B. subtilis* lipid extract. In all cases, the order of FA is as used above.

of the relative quantitation of the isomeric species. Here, standards of 17:0, 16:0(14Me), and 16:0(15Me) were prepared as binary and ternary mixtures of varying ratios to investigate the quantitation capabilities. Figure 5 reflects data obtained from 1:1 binary mixtures of the standards that were prepared to a FA final concentration of 10 $\mu$M in each experiment. Fractional ion abundances are plotted over the $m/z$ range of 440−524, which encompasses the most diagnostic product ions, obtained under conditions in which the precursor ions at $m/z$ 538 were largely depleted. Fractional abundances were calculated by normalizing all product ions. Predicted fractional abundances for the listed $m/z$'s were calculated via linear combination of results of the pure standards. In all three plots (Figure 5A−C), the predicted values exceeded the measured fractional abundances. Notably, Figure 5A and Figure 5C, which represent 1:1 mixtures of 17:0 and 16:0(14Me) and 16:0(14Me) and 16:0(15Me), respectively, reflect predictions that exceed measurements more so than in Figure 5B (1:1 mixture of 17:0 and 16:0(15Me)). This may indicate that 16:0(14Me) is lower in concentration than is believed and/or has decreased relative ionization efficiency. Otherwise, there is reasonable agreement between the measured and predicted fractional abundances, indicating that this method may be able to offer relative quantitation. Further binary mixtures are shown in Figure S14 and ternary mixtures are shown in Figure S15 of various ratios where the total FA concentration was consistently prepared to 10 $\mu$M. In the case of ternary mixtures (Figure S15), the titles reflect ratios of each FA in order of 17:0:16:0(14Me):16:0(15Me). Generally, predicted fractional abundances of all mixtures are overestimated when compared to the measured fractional abundances. Nevertheless, the predicted fractional abundances correlate with changes in relative contributions of the different isomers, indicating that relative quantitative information can be obtained.


https://doi.org/10.1021/acs.analchem.3c04510
Anal. Chem. 2024, 96, 3389−3401

Bacterial membrane lipids, such as those in *Staphylococcus aureus*[87] and *Bacilis subtilis* (*B. subtilis*[88]), are reported to contain large amounts of branching that play key roles in bacterial growth and membrane fluidity.[89] Here, a lipid extract of *B. subtilis* was prepared as described above and directly injected into the mass spectrometer using negative mode nESI. The MS1 of the extract is shown in Figure 6A with a zoom in of the $m/z$ 267−272 region in Figure 6B.

At less than 2% relative abundance, the ions giving rise to $m/z$ 269.2 are consistent with FA 17:0 or any of its branched counterparts. Ions at this $m/z$ were mass selected and subjected to the ion/ion reaction described above and subjected to CID to drive off TEMPO to generate the radical species, which was further mass isolated and subjected to CID (Figure 6C). The fragmentation patterns are reminiscent of those shown in Figure 2, which tentatively confirm that the ion isolated from the extract was indeed a fatty acid. Furthermore, there are ions with increased abundance relative to those generated from the straight-chain isomer that are consistent with the prominent ions related to the branched isomers in Figure 2. Specifically, ions at $m/z$ 469 and 482 with increased abundances are observed that relate to 16:0(14Me), and ions at $m/z$ 483 and 496 are observed at elevated abundances that relate to 16:0(15Me), which suggests the presence of both isomers in this extract. The ions at $m/z$ 483 and 496 are considerably higher than those at $m/z$ 469 and 482, which can indicate that 16:0(15Me) is more abundant in the extract than the other branched isomer. Further evidence supporting this is the decreased abundance of $m/z$ 510, which is also observed for 16:0(15Me).

To further investigate, Figure 7 reflects data derived from the ternary mixtures shown in Figure S15 with the fractional abundances calculated from the anion isolated from the *B. subtilis* lipid extract. The diagnostic ions for 16:0(15Me) are even more abundant in the *B. subtilis* sample than when 16:0(15Me) made up 50% of the standard mixture (the highest fraction examined with the standards). This indicates that the major component of over 50% of the unknown from the *B. subtilis* extract is likely 16:0(15Me). The 16:0(14Me) isomer is also present, based on the elevated signals at $m/z$ 469 and 482, and potentially 17:0 as well, as the minor components. Further in-depth experimental and statistical analysis is needed to make a more precise determination of the percentages of each isomer, although generally there is strong evidence that a BCFA was found in a lipid extract of *B. subtilis* with 16:0(15Me) being the major component compared to isomeric 16:0(14Me) and 17:0.

## CONCLUSIONS

In this work, we describe a gas-phase charge switching reagent that can charge and invert a fatty acid anion to a radical cation species that undergoes RDD upon CID. RDD is particularly useful in localizing branching sites in fatty acids and fatty acid esters. The ion−ion reaction approach can be applied equally well to fatty acid anions generated via ESI or via gas-phase fragmentation of lipid anions containing fatty acid esters. Specifically, deprotonated FAs are converted to cations via the attachment of a divalent magnesium Terpy-TEMPO complex to produce a $[FA - H + (Terpy\text{-}TEMPO)\text{-}Mg^{2+}]^+$ cation. Ion trap CID of the cationic complex results in a homolytic cleavage and loss of the TEMPO moiety leaving behind a nascent free radical site, $[FA - H + Mg^{2+}\text{-}Terpy\text{-}CH_2^{\cdot}]^+$. Further interrogation with CID of the $[FA - H + Mg^{2+}\text{-}Terpy\text{-}CH_2^{\cdot}]^+$ ion results in localization of the site(s) of branching. The ion−ion reaction approach is able to identify if and where branching is present. During the course of the work, it was noted that the relative abundances of odd-electron product ions, some of which are informative of branching, are highly sensitive to activation conditions. An advantage of the use of the TEMPO-derivatized reagent is that the radical can be generated efficiently via the facile loss of TEMPO and subsequently activated under relatively gentle conditions to allow for the generation of the most informative products.

## ASSOCIATED CONTENT

### Supporting Information

The Supporting Information is available free of charge at https://pubs.acs.org/doi/10.1021/acs.analchem.3c04510.

Description and NMR data of the synthesis of Terpy-TEMPO, product ion spectrum of [17:0-H+MgTerpy]+, BT-CID variation demonstrating the transition from RDD to CRF-life product ions, dipolar DC kinetics of odd and even electron product ions, IT-CID of odd and even electron product ions, observed product ions for phytanic acid with various initial radical sites and their mechanisms, and binary and ternary mixture analysis of pure standards (PDF)

## AUTHOR INFORMATION


### Corresponding Authors

Jinshan Gao − *Department of Chemistry and Biochemistry, Montclair State University, Montclair, New Jersey 07043, United States*; Email: gaoj@montclair.edu

Scott A. McLuckey − *Department of Chemistry, Purdue University, West Lafayette, Indiana 47907, United States*; orcid.org/0000-0002-1648-5570; Email: mcluckey@purdue.edu

### Authors

De'Shovon M. Shenault − *Department of Chemistry, Purdue University, West Lafayette, Indiana 47907, United States*

Kimberly C. Fabijanczuk − *Department of Chemistry, Purdue University, West Lafayette, Indiana 47907, United States*

Rayan Murtada − *Department of Chemistry and Biochemistry, Montclair State University, Montclair, New Jersey 07043, United States*

Shane Finn − *Department of Chemistry and Biochemistry, Montclair State University, Montclair, New Jersey 07043, United States*

L. Edwin Gonzalez − *Department of Chemistry, Purdue University, West Lafayette, Indiana 47907, United States*; orcid.org/0000-0002-8207-4075

Complete contact information is available at: https://pubs.acs.org/10.1021/acs.analchem.3c04510


### Author Contributions

D.M.S. engaged in collecting data, planning experiments, and writing the initial draft. K.C.F. engaged in collecting data, planning experiments, and writing and editing aspects of the manuscript. R.M. and S.F. synthesized the TEMPO-Terpy ligand and contributed to planning experiments. L.E.G. prepared the *Bacillus subtilis* sample. S.A.M. and J.G. engaged in planning experiments, interpreting data, and drafting and editing the manuscript.



https://doi.org/10.1021/acs.analchem.3c04510
Anal. Chem. 2024, 96, 3389−3401

### Funding

National Science Foundation CHE-2304386, CHE-2107798, and CHE-2116596.

### Notes

The authors declare no competing financial interest.

## ACKNOWLEDGMENTS

This research was supported by the National Science Foundation under grants CHE-2304386, CHE-2107798, and CHE-2116596. The authors acknowledge SCIEX, and particularly Mr. Frank Londry, for modifying the instruments to enable these ion/ion reaction experiments and Dr. James Hager, also of SCIEX, for helpful discussions.

## REFERENCES

(1) Calder, P. C. *J. Parenter. Enteral. Nutr.* 2015, *39* (1S), 18S−32S.
(2) De Carvalho, C. C. C. R.; Caramujo, M. J. *Molecules* 2018, *23* (10), 2583.
(3) Kaneda, T. *J. Biol. Chem.* 1963, *238* (4), 1229−1235.
(4) Christie, W. W.; Han, X. *Lipid Analysis*; Woodhead Publishing, 2010; Chapter 1.
(5) Kaneda, T. *J. Bacteriol.* 1967, *93* (3), 894−903.
(6) Kaneda, T. *Microbiol. Rev.* 1991, *55* (2), 288−302.
(7) Bishop, D. G.; Rutberg, L.; Samuelsson, B. *Eur. J. Biochem.* 1967, *2* (4), 448−453.
(8) Nickels, J. D.; Chatterjee, S.; Mostofian, B.; Stanley, C. B.; Ohl, M.; Zolnierczuk, P.; Schulz, R.; Myles, D. A. A.; Standaert, R. F.; Elkins, J. G.; Cheng, X.; Katsaras, J. *J. Phys. Chem. Lett.* 2017, *8* (17), 4214−4217.
(9) Oku, H.; Kaneda, T. *J. Biol. Chem.* 1988, *263* (34), 18386−18396.
(10) Hoeger, P. H.; Schreiner, V.; Klaassen, I. A.; Enzmann, C. C.; Friedrichs, K.; Bleck, O. *Br. J. Dermatol.* 2002, *146* (2), 194−201.
(11) Hoeger, P. H.; Schreiner, V.; Klaassen, I. A.; Enzmann, C. C.; Friedrichs, K.; Bleck, O. *Br. J. Dermatol.* 2002, *146* (2), 194−201.
(12) Ran-Ressler, R. R.; Devapatla, S.; Lawrence, P.; Brenna, J. T. *Pediatr. Res.* 2008, *64* (6), 605−609.
(13) Souchier, M.; Joffre, C.; Beynat, J.; Grégoire, S.; Acar, N.; Bretillon, L.; Bron, A. M.; Bourcier, T.; Speeg-Schatz, C.; Creuzot-Garcher, C. *Invest. Ophthalmol. Vis. Sci.* 2008, *49* (13), 2391.
(14) Schönfeld, P.; Kahlert, S.; Reiser, G. *Biochem. J.* 2004, *383* (1), 121−128.
(15) Lheureux, P. E.; Penaloza, A.; Zahir, S.; Gris, M. *Crit. Care* 2005, *9* (5), 431.
(16) Wanders, R. J. A.; Jansen, G. A.; Lloyd, M. D. *Biochim. Biophys. Acta BBA - Mol. Cell Biol. Lipids* 2003, *1631* (2), 119−135.
(17) Rönicke, S.; Kruska, N.; Kahlert, S.; Reiser, G. *Neurobiol. Dis.* 2009, *36* (2), 401−410.
(18) Nanau, R. M.; Neuman, M. G. *Clin. Biochem.* 2013, *46* (15), 1323−1338.
(19) Pham, H. T.; Trevitt, A. J.; Mitchell, T. W.; Blanksby, S. J. *Rapid Commun. Mass Spectrom.* 2013, *27* (7), 805−815.
(20) Blanksby, S. J.; Mitchell, T. W. *Annu. Rev. Anal. Chem.* 2010, *3* (1), 433−465.
(21) Chiu, H.-H.; Kuo, C.-H. *J. Food Drug Anal.* 2020, *28* (1), 60−73.
(22) He, L.; Prodhan, M. A. I.; Yuan, F.; Yin, X.; Lorkiewicz, P. K.; Wei, X.; Feng, W.; McClain, C.; Zhang, X. *J. Chromatogr. B* 2018, *1092*, 359−367.
(23) Christie, W. W. *Lipids* 1998, *33* (4), 343−353.
(24) Wang, Z.; Wang, D. H.; Park, H. G.; Tobias, H. J.; Kothapalli, K. S. D.; Brenna, J. T. *Anal. Chem.* 2019, *91* (23), 15147−15154.
(25) Wang, D. H.; Wang, Z.; Brenna, J. T. *J. Agric. Food Chem.* 2020, *68* (17), 4973−4980.
(26) Zirrolli, J. A.; Murphy, R. C. *J. Am. Soc. Mass Spectrom.* 1993, *4* (3), 223−229.
(27) Harvey, D. J. *Biomed. Mass Spectrom.* 1982, *9* (1), 33−38.
(28) Chiu, H.-H.; Kuo, C.-H. *J. Food Drug Anal.* 2020, *28* (1), 60−73.
(29) Hsu, F.-F.; Turk, J. *Journal of Chromatography B* 2009, *877* (26), 2673−2695.
(30) Han, X.; Gross, R. W. *J. Am. Soc. Mass Spectrom.* 1995, *6* (12), 1202−1210.
(31) Han, X.; Gross, R. W. *J. Lipid Res.* 2003, *44* (6), 1071−1079.
(32) Pulfer, M.; Murphy, R. C. *Mass Spectrom. Rev.* 2003, *22* (5), 332−364.
(33) Murphy, R. C.; Gaskell, S. J. *J. Biol. Chem.* 2011, *286* (29), 25427−25433.
(34) Wenk, M. R. *Nat. Rev. Drug Discov* 2005, *4* (7), 594−610.
(35) Li, L.; Han, J.; Wang, Z.; Liu, J.; Wei, J.; Xiong, S.; Zhao, Z. *Int. J. Mol. Sci.* 2014, *15* (6), 10492−10507.
(36) Harkewicz, R.; Dennis, E. A. *Annu. Rev. Biochem.* 2011, *80* (1), 301−325.
(37) Han, X. *Biochim. Biophys. Acta BBA -Mol. Cell Biol. Lipids* 2010, *1801* (8), 774−783.
(38) Guttenplan, K. A.; Weigel, M. K.; Prakash, P.; Wijewardhane, P. R.; Hasel, P.; Rufen-Blanchette, U.; Munch, A. E.; Blum, J. A.; Fine, J.; Neal, M. C.; Bruce, K. D.; Gitler, A. D.; Chopra, G.; Liddelow, S. A.; Barres, B. A. *Nature* 2021, *599* (7883), 102−107.
(39) Gross, M. L. *Int. J. Mass Spectrom.* 2000, *200* (1), 611−624.
(40) Kerwin, J. L.; Wiens, A. M.; Ericsson, L. H. *J. Mass Spectrom.* 1996, *31* (2), 184−192.
(41) Jensen, N. J.; Gross, M. L. *Lipids* 1986, *21*, 362−365.
(42) McLuckey, S. A.; Mentinova, M. *J. Am. Soc. Mass Spectrom.* 2011, *22* (1), 3−12.
(43) Randolph, C. E.; Blanksby, S. J.; McLuckey, S. A. *Chem. Phys. Lipids* 2020, *232*, No. 104970.
(44) Bollinger, J. G.; Thompson, W.; Lai, Y.; Oslund, R. C.; Hallstrand, T. S.; Sadilek, M.; Turecek, F.; Gelb, M. H. *Anal. Chem.* 2010, *82* (16), 6790−6796.
(45) Yang, W. C.; Adamec, J.; Regnier, F. E. *Anal. Chem.* 2007, *79* (14), 5150−5157.
(46) Bollinger, J. G.; Rohan, G.; Sadilek, M.; Gelb, M. H. *J. Lipid Res.* 2013, *54* (12), 3523−3530.
(47) Yang, K.; Dilthey, B. G.; Gross, R. W. *Anal. Chem.* 2013, *85* (20), 9742−9750.
(48) Wang, M.; Han, R. H.; Han, X. L. *Anal. Chem.* 2013, *85* (19), 9312−9320.
(49) Liu, X. P.; Moon, S. H.; Mancuso, D. J.; Jenkins, C. M.; Guan, S. P.; Sims, H. F.; Gross, R. W. *Anal.l Biochem.* 2013, *442* (1), 40−50.
(50) Tatituri, R. V. V.; Wolf, B. J.; Brenner, M. B.; Turk, J.; Hsu, F.-F. *Anal. Bioanal. Chem.* 2015, *407*, 2519−2528.
(51) Pham, H. T.; Ly, T.; Trevitt, A. J.; Mitchell, T. W.; Blanksby, S. J. *Anal. Chem.* 2012, *84* (17), 7525−7532.
(52) Pham, H. T.; Trevitt, A. J.; Mitchell, T. W.; Blanksby, S. J. *Rapid Commun. Mass Spectrom.* 2013, *27* (7), 805−815.
(53) Narreddula, V. R.; Boase, N. R.; Ailuri, R.; Marshall, D. L.; Poad, B. L. J.; Kelso, M. J.; Trevitt, A. J.; Mitchell, T. W.; Blanksby, S. J. *Anal. Chem.* 2019, *91* (15), 9901−9909.
(54) Narreddula, V. R.; McKinnon, B. I.; Marlton, S. J. P.; Marshall, D. L.; Boase, N. R. B.; Poad, B. L. J.; Trevitt, A. J.; Mitchell, T. W.; Blanksby, S. J. *Analyst* 2021, *146* (1), 156−169.
(55) Pham, H. T.; Julian, R. R. *Analyst* 2016, *141* (4), 1273−1278.
(56) Zhao, X.; Wu, G.; Zhang, W.; Dong, M.; Xia, Y. *Anal. Chem.* 2020, *92* (21), 14775−14782.
(57) Zhao, X.; Xia, Y. *J. Am. Soc. Mass Spectrom.* 2021, *32* (2), 560−568.
(58) Lin, Q.; Li, P.; Jian, R.; Xia, Y. *J. Am. Soc. Mass Spectrom.* 2022, *33* (4), 714−721.
(59) Randolph, C. E.; Beveridge, C. H.; Iyer, S.; Blanksby, S. J.; McLuckey, S. A.; Chopra, G. *J. Am. Soc. Mass Spectrom.* 2022, *33* (11), 2156−2164.
(60) Li, P.; Hoffmann, W. D.; Jackson, G. P. *Int. J. Mass Spectrom.* 2016, *403*, 1−7.
(61) Chao, H.-C.; McLuckey, S. A. *Trends Analyt. Chem.* 2023, *158*, No. 116852.

(62) Randolph, C. E.; Foreman, D. J.; Blanksby, S. J.; McLuckey, S. A. *Anal. Chem.* 2019, *91* (14), 9032−9040.
(63) Randolph, C. E.; Foreman, D. J.; Betancourt, S. K.; Blanksby, S. J.; McLuckey, S. A. *Anal. Chem.* 2018, *90* (21), 12861−12869.
(64) Randolph, C. E.; Blanksby, S. J.; McLuckey, S. A. *Anal. Chem.* 2020, *92* (1), 1219−1227.
(65) Shenault, D. M.; McLuckey, S. A.; Franklin, E. T. *J. Mass Spectrom.* 2023, *58*, No. e4913.
(66) Randolph, C. E.; Shenault, D. M.; Blanksby, S. J.; McLuckey, S. A. *J. Am. Soc. Mass Spectrom.* 2021, *32*, 455−464.
(67) Gaspar, K.; Fabijanczuk, K.; Otegui, T.; Acosta, J.; Gao, J. *J. Am. Soc. Mass Spectrom.* 2019, *30* (3), 548−556.
(68) Gao, J.; Thomas, D. A.; Sohn, C. H.; Beauchamp, J. L. *J. Am. Chem. Soc.* 2013, *135* (29), 10684−10692.
(69) Murtada, R.; Fabijanczuk, K.; Gaspar, K.; Dong, X.; Alzareni, K. Z.; Calix, K.; Manniquez, E.; Bakestani, R. M.; Kenttämaa; Gao, J. *Anal. Chem.* 2020, *92* (20), 13794−13802.
(70) Hsu, F.-F. *Anal Bioanal Chem.* 2018, *410* (25), 6387−6409.
(71) Liebisch, G.; Vizcaíno, J. A.; Köfeler, H.; Trötzmüller, M.; Griffiths, W. J.; Schmitz, G.; Spener, F.; Wakelam, M. J. O. *J. Lipid Res.* 2013, *54* (6), 1523−1530.
(72) Shinpuku, Y.; Inui, F.; Nakai, M.; Nakabayashi, Y. *J. Photochem. Photobiol., A* 2011, *222*, 203−209.
(73) Schneider, T.; Gavrilova, I.; Budisa, N. *Tetrahedron Lett.* 2019, *60*, 906−910.
(74) Gao, J.; Thomas, D. A.; Sohn, C. H.; Beauchamp, J. L. *J. Am. Chem. Soc.* 2013, *135* (29), 10684−10692.
(75) Yang, Y.; Yin, Y.; Chen, X.; Chen, C.; Xia, Y.; Qi, H.; Baker, P. N.; Zhang, H.; Han, T.-L. *Sci. Rep.* 2019, *9* (1), 12017.
(76) Bhanot, J. S.; Fabijanczuk, K. C.; Abdillahi, A. M.; Chao, H.-C.; Pizzala, N. J.; Londry, F. A.; Dziekonski, E. T.; Hager, J. W.; McLuckey, S. A. *Int. J. Mass Spectrom.* 2022, *478*, No. 116874.
(77) Xia, Y.; Liang, X.; McLuckey, S. A. *J. Am. Soc. Mass Spectrom.* 2005, *16* (11), 1750−1756.
(78) Blanksby, S. J.; Ellison, G. B. *Acc. Chem. Res.* 2003, *36*, 255−263.
(79) Namysl, S.; Pelucchi, M.; Herbinet, O.; Frassoldati, A.; Faravelli, T.; Battin-Leclerc, F. A. *Chem. Eng. J.* 2019, *373*, 973−984.
(80) Xia, Y.; Chrisman, P. A.; Pitteri, S. J.; Erickson, D. E.; McLuckey, S. A. *J. Am. Chem. Soc.* 2006, *128*, 11792−11798.
(81) Silzel, J. W.; Julian, R. R. *J. Am. Soc. Mass Spectrom.* 2023, *34* (3), 452−458.
(82) Mehnert, S. A.; Fischer, J. L.; McDaniel, M. R.; Fabijanczuk, K. C.; McLuckey, S. A. *J. Am. Soc. Mass Spectrom.* 2023, *34*, 1166−1174.
(83) Hsu, F.-F.; Turk, J. *J. Am. Soc. Mass Spectrom.* 2000, *11* (10), 892−899.
(84) Jordan, S. F.; Nee, E.; Lane, N. *Interface Focus* 2019, *9* (6), No. 20190067.
(85) Malik, S.; Liu, C.-G.; Zhao, X.-Q.; Mehmood, M. A. Long-Chain Liquid Biofuels. In *Comprehensive Biotechnology*, 3rd ed.; Moo-Young, M., Ed.; Pergamon: Oxford, 2019; pp 101−109.
(86) Koga, Y. *J. Mol. Evol.* 2011, *72* (3), 274−282.
(87) Tiwari, K.; Gatto, C.; Wilkinson, B. *Molecules* 2018, *23* (5), 1201.
(88) Kaneda, T. *J. Biol. Chem.* 1963, *238* (4), 1222−1228.
(89) Kaneda, T. *Microbiological Reviews* 1991, *55* (2), 288−302.


https://doi.org/10.1021/acs.analchem.3c04510
*Anal. Chem.* 2024, 96, 3389−3401